Available online at www.sciencedirect.com
ScienceDirect
Separation and Purification Technology 52 (2006) 126–135
Separation Purification Technology
www.elsevier.com/locate/seppur

The deposition morphology of Brownian particles onto a spherical collector

You-Im Chang *, Lee Rong-Shin, Cheng Wei-You

Department of Chemical Engineering, Tunghai University, Taichung 40704, Taiwan, Republic of China

Received 30 December 2005; received in revised form 27 March 2006; accepted 27 March 2006

Abstract

The deposition morphology of particles onto a spherical collector is investigated by applying the Brownian dynamics simulation method in the present paper. The effect of various types of the total interaction energy curves of DLVO theory, and of the shadow area cast by those deposited particles, on the particles' collection efficiencies are examined. The simulation results show that the collection efficiency is always higher when the particle's Brownian motion behavior is taken into consideration. As the deposition location moves closer to the front stagnation point of the collector, the dendrites formed by those Brownian particles also contain more particles. The present simulation method successfully describes the amount of particles collected as well as the morphology of the deposits in a detailed step-by-step manner.

Keywords: Deposition; Morphology; Brownian particle; DLVO theory; Filtration

1. Introduction

The importance of knowing the morphology of particle deposits is obvious in determining the collection efficiency of a fixed bed granular filter. Since the formation and growth of particle deposits changes the surface characteristics of individual collectors continuously in a deep bed filter, hence the extent of particle deposition profoundly affects the rate of particle retention and makes the filtration process become time dependent. Tien et al. [1] and Wang et al. [2] had outlined a direct approach for analyzing the deposition morphology of particles from a flowing suspension to a collector. In their approach, the particle deposition was examined by tracking the trajectories of individual particles as they move toward the collector. Beizaie et al. [3] then executed this approach successfully with the establishment of a comprehensive simulation procedure. In their simulation, Wang et al. [2] had considered the deposition process as an interplay of two basic concepts, the shadow effect caused by those deposited particles and the random distribution of particles in the suspension, which are intrinsic to all particles in a suspension flowing past a collector. The results of their study provide not only the deposition rate of entire filtration period but also relevant information on the geometry of the deposits formed time dependently. The simulation procedure can be found in detail elsewhere ([4], see Chapter 8 of Tien Chi's book) and will be adopted in the present paper.

The trajectory equations formulated by Wang et al. [2] and Beizaie et al. [3], which take into account the hydrodynamic and electrokinetic forces, were proven to be able to describe the deposition morphology of colloidal particles onto the collector surfaces. Since the Brownian diffusion force was not considered in those earlier works, the force balance equations established by their trajectory analyses were deterministic. However, if the Brownian diffusion forces are the dominant force of the deposition process, the deterministic calculation of particle trajectory is no longer possible. Inclusion of these Brownian random forces in the Lagrangian type force balance equation leads to a Langevin type equation, which was solved successfully by Kanaoka et al. [5] in their simulation model of aerosol filtration. Their Brownian dynamics simulation method was proved useful when the inertia and long-range forces (i.e. van der Waals attraction and electrical double layer repulsion) are of the same order of the Brownian diffusion force [6,7]. Applying with this dynamics method, a stochastic procedure was established successfully in our previous papers to simulate the initial deposition rates of Brownian particles onto a spherical collector [8] and in the con-

* Corresponding author.
E-mail address: yichang@thu.edu.tw (Y.-I. Chang).

1383-5866/$ – see front matter © 2006 Elsevier B.V. All rights reserved.
doi:10.1016/j.seppur.2006.03.030

stricted tube model [9], respectively. The results obtained by those papers showed that the height of the primary maximum and the depth of the secondary minimum in the total interaction energy curve of DLVO theory [10] play important roles in determining the collection efficiency of Brownian particles at low Reynolds numbers.

In addition to considering the Brownian diffusion effect, the concept of the control window located far upstream from the collector will be adopted in the present paper, too. This control window can be considered as the place where the approaching particles originate singularly and randomly (see Fig. 1) [2,3]. In other words, the probability of finding a particle's location within this control window is the same as in any other locations within the window. By knowing the initial positions of those particles within the control window and the flow field around the collector, one can then determine the particle deposition morphology by integrating the trajectory equation and the collection efficiency of the collector consequently. The simulation results obtained by Beizaie et al. [3] and Ramarao et al. [7] indicate that the deposition process consists of three stages: the clean collector stage, the dendrite growth stage and the final individual dendrites joined stage. Depending upon the size of the control window (i.e. the original number of particles), they also found that the number of dendrites formed will remain the same at the final stage, which implies that the collection efficiency is a time dependent function and will remain unchanged when the final stage of filtration is achieved. Moreover, the lengths of these three stages were found to be dependent on the relative particle to collector size, the flow field around the collector and the electrostatic forces of the DLVO theory.

By using the same simulation procedure established by Beizaie et al. [3] and Ramarao et al. [7] and Langevin type trajectory equation, the deposition morphology of Brownian particles onto a spherical collector will be investigated in the present paper. In these simulations, the effects of the various shapes of the total interaction energy curves of DLVO theory and the shadow effect are also considered. Distinguished deposition morphology is found between those particles with and without considering the Brownian diffusion behavior.

2. Theoretical formulation

As shown in Fig. 1, assume that there is a square 2b by 2b dimension control window, whose center is perpendicularly located on the y-axis far upstream from the collector. This control window can be considered as the spatial domain through which particles originate singularly and randomly. The distribution of the initial positions of each approaching particle is assigned by the random number software of IMSL [11] in the present simulation. With the specification of the flow field around the collector, the particle's deposition trajectory by integrating the Langevin type equation can be simulated. From the trajectory of a given particle, one can then determine whether this particle will be deposited onto the surfaces of a collector or onto the previously deposited particle.

Let S be the area of the control window, the number of particles passing through this control window for a time t is

$$M = SU_\infty C_\infty t \tag{1}$$

where U_∞ and C_∞ are the approach velocity and concentrations of the suspension.

If m is the number of particles collected as a function of M, then

$$m = \int_0^t SU_\infty C_\infty \eta \, \mathrm{d}t \tag{2}$$

From Eqs. (1) and (2), one can express the collection efficiency of the collector as

$$\eta = \frac{\mathrm{d}m}{\mathrm{d}M} \tag{3}$$

On the other hand, if the collector is assumed to be spherical in shape, the extent of particle deposition is expressed by the single collector efficiency η_s which can be written as

$$\eta_s = \frac{1}{\pi r_f^2 U_\infty C_\infty}\frac{\mathrm{d}m}{\mathrm{d}t} = \frac{S}{\pi r_f^2}\frac{\mathrm{d}m}{\mathrm{d}M} = \frac{\mathrm{d}m}{\mathrm{d}M^*},$$

$$\text{with } M^* = M(r_f^2/S) \tag{4}$$

where r_f is the radius of the spherical collector. In the present paper, the relationship between m and M^* will be investigated

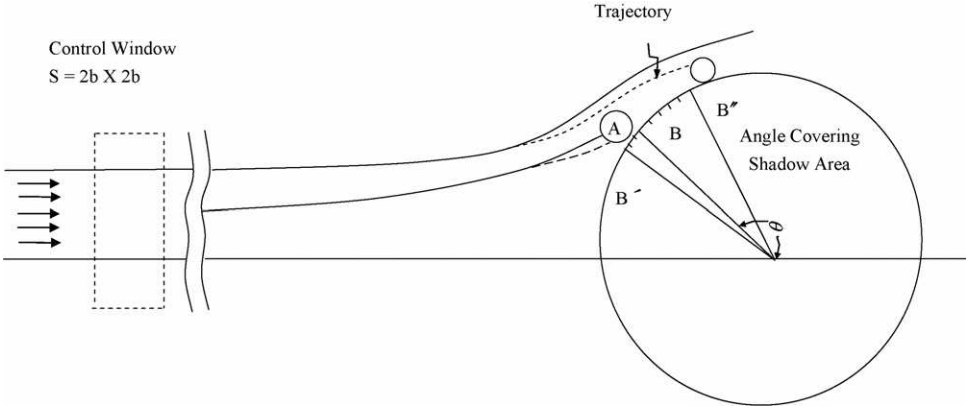

Fig. 1. The schematic diagram of the control window for simulating deposition of Brownian particles onto a spherical collector, in which the concept of shadow area is illustrated.

in order to obtain information on the increase of collection efficiency as a function of the extent of particle deposition.

For simplicity, the creeping flow field around the spherical collector in two-dimensional cylindrical coordinates is adopted in the present paper. The velocity components U_r and U_θ are

$$U_r = U_\infty \left(1 - \frac{R^2}{r^2}\right) \cos\theta \tag{5}$$

$$U_\theta = -U_\infty \left(1 + \frac{R^2}{r^2}\right) \sin\theta \tag{6}$$

In the present paper, the Langevin trajectory equation describing the force balance on a Brownian particle with radius a_p is written as:

$$m_p \frac{d\vec{V}}{dt} = F_d + F_e + F_r \tag{7}$$

where m_p is the mass of the particle, $\vec{V}$ the particle velocity vector and t is the time. The forces considered in the present paper are the drag force F_d, the external force F_e and the random force F_r. The trajectory of a Brownian particle described by the above Langevin equation can be obtained incrementally. Over a sufficiently short time interval, $0 < t < \Delta t$, the fluid velocity U_r and U_θ in Eqs. (5) and (6) can be regarded as constant. Then, the particle velocity vector can be represented as [8,9]

$$V = \left\{ \left[V_0 e^{-\beta t} + U(1 - e^{-\beta t}) \right] F_2(H) + R_v(t) + \frac{1}{\beta} \left(\frac{F_{LO} + F_{DL}}{m_p} \right) (1 - e^{-\beta t}) \right\} F_1(H) F_3(H) \tag{8}$$

with

$$R_V(t) = \int_0^t e^{\beta(\zeta - t)} A(\zeta)\, d\zeta$$

where V_0 is the initial velocity of particles, m_p the mass of the particle, U the fluid velocity vector, β the friction coefficient per unit mass of particle, and $F_1(H)$, $F_2(H)$, and $F_3(H)$ are the retardation factors of normal vector, drag force, and shear vector, respectively. Substituting dZ/dt for V with the initial condition $S = S_0$ at $t = 0$, the trajectory equation of particles can be expressed as:

$$Z = Z_0 + \left\{ \frac{V_0}{\beta}(1 - e^{-\beta t}) + U \left[t - \frac{1}{\beta}(1 - e^{-\beta t}) \right] \right\} \times F_1(H) F_2(H) F_3(H) + \left\{ R_r(t) + \left(\frac{F_{LO} + F_{DL}}{\beta m_p} \right) (t + \frac{e^{-\beta t}}{\beta} - \frac{1}{\beta}) \right\} \times F_1(H) F_3(H) \tag{9}$$

with

$$R_r(t) = \int_0^t \left[\int_0^n e^{\beta\zeta} A(\zeta)\, d\zeta \right] e^{-\beta n}\, dn$$

where $A(t)$ represents a Gaussian white noise process in stochastic terms. $R_v(t)$ and $R_r(t)$ are two random deviates which are bivariate Gaussian distribution. The details of $R_v(t)$ and $R_r(t)$ can be found in Kanaoka et al. [5] and Ramarao et al. [7]. Note that the value of the time step Δt adopted in the present paper remains as small as 10^{-6} s, which is the same order of the momentum relaxation time ($\sim 1/\beta$) of the particle [6].

In Eqs. (8) and (9), F_{LO} and F_{DL} are the van der Waals force and the electrostatic repulsion force interacting between the particle and the collector surface, respectively.

$$F_{LO} = -\nabla\phi_{LO}, \quad F_{DL} = -\nabla\phi_{DL} \tag{10}$$

with

$$\phi_{LO} = -N_{LO} \left[\frac{2(H+1)}{H(H+2)} + \ln H - \ln(H+2) \right]$$

(with the unit of $k_B T$)

$$\phi_{DL} = N_{E1} \left\{ N_{E2} \ln \left[\frac{1 + \exp(-X)}{1 - \exp(-X)} \right] + \ln \left[1 - \exp(-2X) \right] \right\}$$

(with the unit of $k_B T$)

hence:

$$F_{LO} = -\frac{2A}{3r_p} \left[\frac{1}{(H^2 + 2H)^2} \right] \tag{11}$$

$$F_{DL} = \frac{2k_B T}{r_p} N_{E1} (N_{DL}\, e^{-N_{DL} H}) \left\{ \frac{N_{E2} - e^{-N_{DL} H}}{1 - e^{-2N_{DL} H}} \right\} \tag{12}$$

where $H = h_s/r_p$, $N_{LO} = A/6k_B T$, $N_{DL} = \kappa r_p$, $X = N_{DL} H$, $N_{E1} = \nu r_p(\varphi_1^2 + \varphi_2^2)/4k\ T$, $N_{E2} = 2(\varphi_1/\varphi_2)/[1 + (\varphi_1/\varphi_2)^2]$.

In the above equation, h_s is the smallest separation distance between the particle and the collector surface, A the Hamaker constant, k_B the Boltzmann constant, T the absolute temperature, κ the reciprocal of the electric double layer thickness, ν the dielectric constant of the fluid, and φ_1 and φ_2 are the surface (zeta) potentials of the particle and the collector, respectively. The algebraic sum of the van der Waals and double-layer potentials gives the total interaction energy curve of the DLVO theory (i.e. $V_T/k_B T = \phi_{LO} + \phi_{DL}$). In the present paper, the effects of the four types of interaction energy curves [12] on the collection efficiencies of Brownian particles will be investigated. As shown in Fig. 2, curves A exhibits a large primary maximum and a deep secondary minimum; curve B displays a large primary maximum and a negligible secondary minimum; while curve C owns a deep secondary minimum only and a "barrierless" interaction energy curve is represented by curve D. In this figure, $N_{E1} = 105.0$ and $N_{DL} = 10.75$ for curve A, $N_{E1} = 50.0$ and $N_{DL} = 5.02$ for curve B, $N_{E1} = 77.0$ and $N_{DL} = 10.0$ for curve C, $N_{E1} = 0.0$ and $N_{DL} = 0.0$ for curve D, and $N_{E2} = 1.0$ and $N_{LO} = 7.0$ for all four curves. Corresponding to these four types of interaction energy curves with the defined values of N_{E1}, N_{E2}, N_{LO} and N_{DL}, the simulation results of the collection efficiencies ηs and the deposition morphology of particles at various values of M^* (see Eq. (4)) will be given below.

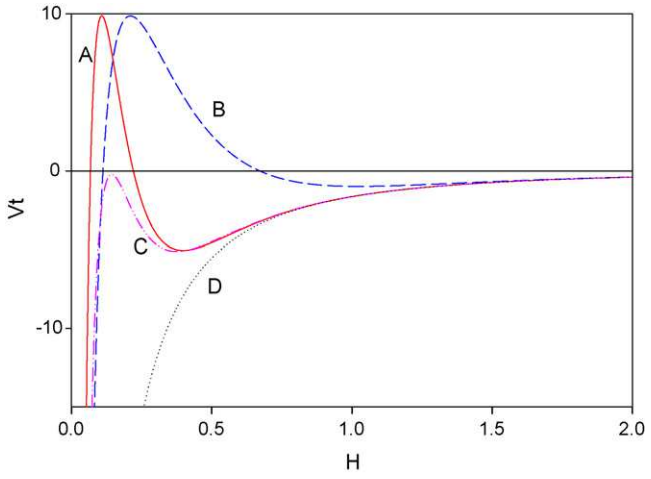

Fig. 2. Four types of total interaction energy curves adopted in the simulation of the present paper, at which $N_{E1} = 105.0$ and $N_{DL} = 10.75$ for curve A, $N_{E1} = 50.0$ and $N_{DL} = 5.02$ for curve B, $N_{E1} = 77.0$ and $N_{DL} = 10.0$ for curve C, $N_{E1} = 0.0$ and $N_{DL} = 0.0$ for curve D, and $N_{E2} = 1.0$ and $N_{LO} = 7.0$ for all four curves.

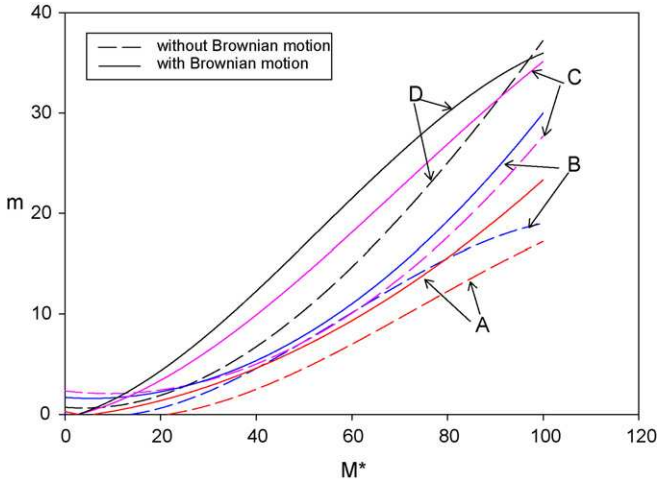

Fig. 3. Simulation results of m vs. M^*, where the dashed lines represent the case when the Brownian motion behavior of particles is not considered and the solid lines represent the case when the Brownian motion behavior of particles is considered.

3. Shadow effect

The shadow effect arises from the fact that once a particle of finite size is deposited on a collector's surface, as illustrated by the arc $B'B''$ shown in Fig. 1, it creates a shadow area around itself within which no subsequent particle deposition can take place. The creation of a shadow area by deposited particles has two consequences [2]. First, because there is no deposition occurring in the shadow area, a discrete site deposition will result along the collector's surface. If the shadow areas occupy most surface area of the collector, then those deposited particles cannot be in the form of a smooth and uniform coating. Secondary, instead of depositing within the shadow area, those subsequent approaching particles now would attach themselves to the deposited particles. This behavior results in the formation of chainlike dendrites as observed in the experimental work of Payatakes et al. [13]. The dendritic growth of those deposited particles indicates that the morphology of particle deposits changes continuously during filtration.

The magnitude of the shadow area is a function of the location of the deposited particle and other parameters shown in the above trajectory equations. The calculations made by Wang et al. [2] for Stokes flow around a spherical collector showed that the magnitude of the shadow area is strongly dependent on the position of deposition, the Stokes number and the relative size ratio N_R between the particle and the collector. The shadow area is shown to increase as the position of deposition moves away from the front stagnation point of the collector, and also increases as the relative size ratio increases.

Table 1
Parameter values adopted in the theoretical simulations of the present paper

Parameters	Ranges
N_{E1}	$0–10^3$
N_{E2}	-1 to 1
N_{LO}	10^{-3} to 10^2
N_{DL}	$5–10^2$
K_B	1.38×10^{-16} erg K^{-1}
ε	0.39
μ	1 cp
T	293 K
ρ_f	1.0 g cm^{-3}
ρ_p	1.0 g cm^{-3}
d_f	100 μm
d_p	1 μm

Table 2
The collection efficiencies corresponding to different M^* for those results obtained in Fig. 3 when the Brownian motion behavior of particles is not considered

M^*	A	B	C	D
20	0.025	0.025	0.025	0.075
30	0.025	0.050	0.125	0.125
40	0.025	0.100	0.175	0.175
50	0.100	0.175	0.175	0.225
60	0.175	0.300	0.300	0.350
70	0.300	0.300	0.300	0.375
80	0.300	0.375	0.375	0.750
90	0.325	0.450	0.500	0.825
100	0.450	0.475	0.825	0.875

Table 3
The collection efficiencies corresponding to different M^* for those results obtained in Fig. 3 when the Brownian motion behavior of particles is considered

M^*	A	B	C	D
20	0.025	0.100	0.075	0.100
30	0.075	0.125	0.150	0.150
40	0.100	0.150	0.225	0.350
50	0.150	0.175	0.350	0.425
60	0.250	0.250	0.525	0.575
70	0.325	0.400	0.575	0.625
80	0.400	0.400	0.600	0.750
90	0.475	0.600	0.775	0.800
100	0.575	0.800	0.900	0.925

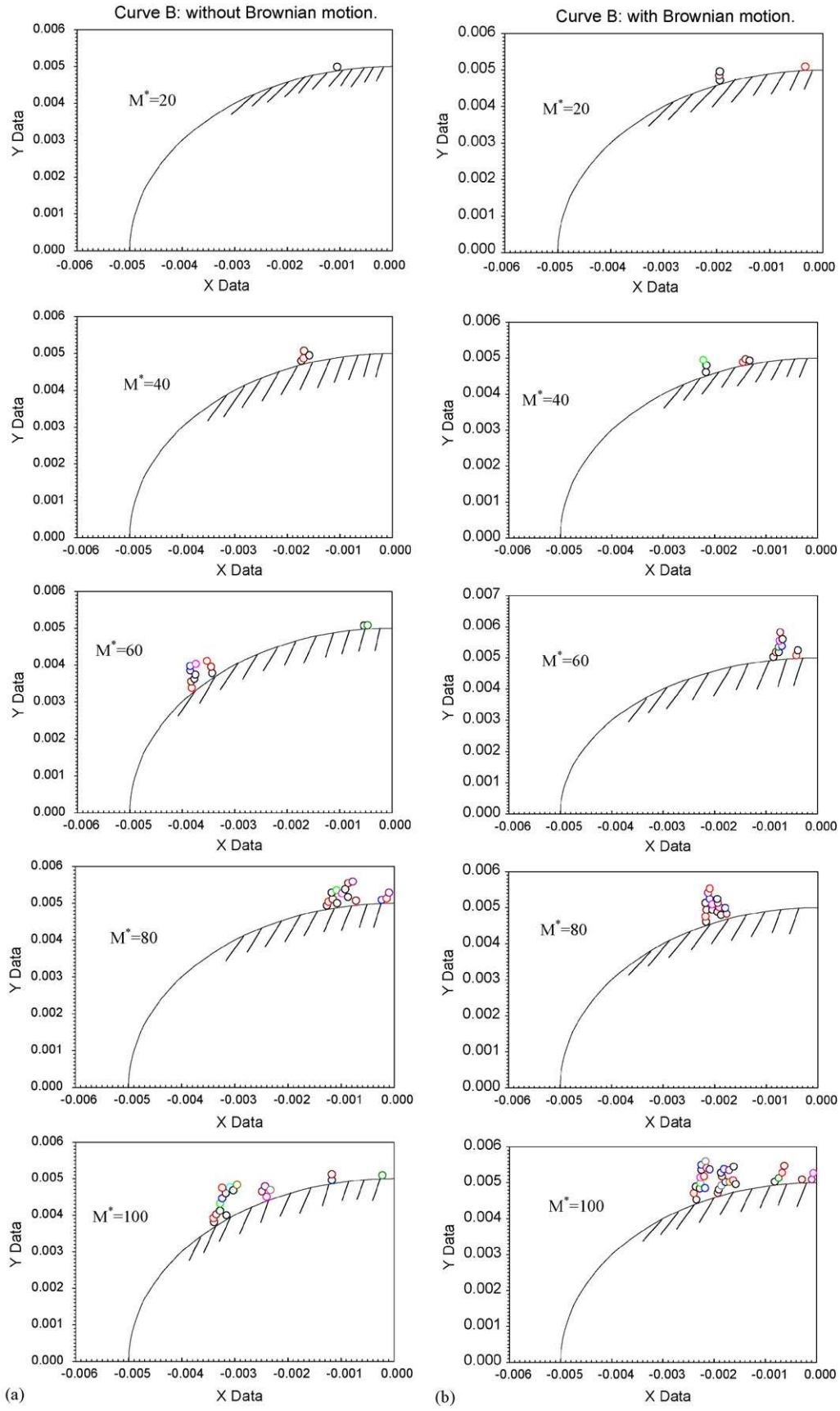

Fig. 4. Simulations results of the deposition morphology of particles for the interaction energy curve B: (a) when the Brownian motion behavior of particles is not considered and (b) when the Brownian motion behavior of particles is considered.

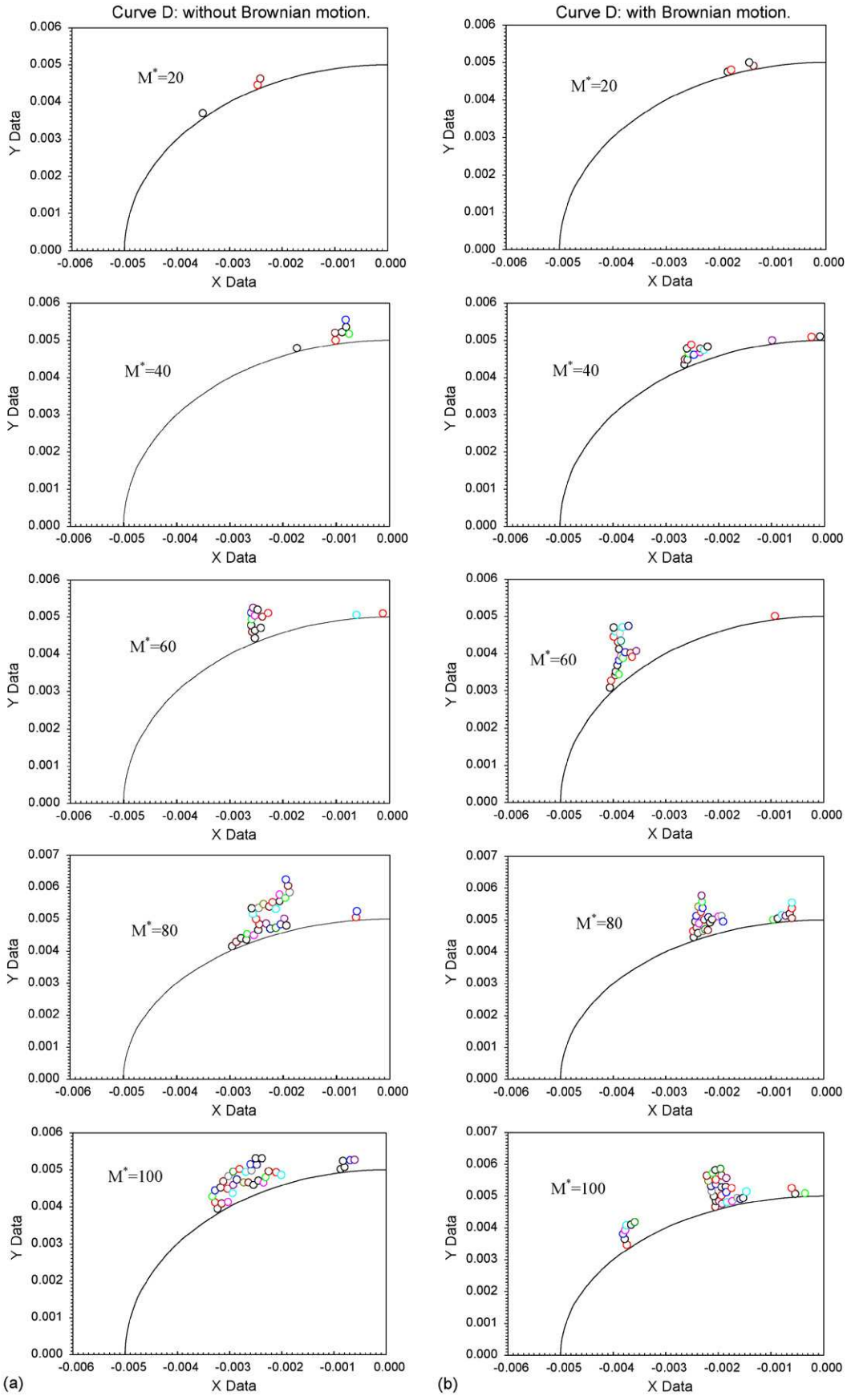

Fig. 5. Simulations results of the deposition morphology of particles for the interaction energy curve D: (a) when the Brownian motion behavior of particles is not considered and (b) when the Brownian motion behavior of particles is considered.

In the present paper, by applying with the Brownian dynamics simulation method mentioned above, the effects of various shapes of DLVO interaction energy curves on the formation of dendrites will be examined. By measuring the angle corresponding to the arc $B'B''$ shown in Fig. 1, the magnitude of the shadow area as the function of the deposition location will be determined, too.

4. Numerical simulation and results

The estimation of the collection efficiency from the trajectory equations based on the above stochastic simulation procedures for those four interaction energy curves shown in Fig. 2 are given below. The corresponding electrokinetic data and other simulation parameters are presented in Table 1. Both the cases of considering and without considering the Brownian motion behavior of particles will be investigated as follows.

The simulation results of m versus M^* are shown in Fig. 3, which indicate that the number of particles collected increases with the increase of M^* (or with the decrease of the size of the control window S through Eq. (4)) for all of those four interaction energy curves shown in Fig. 2 regardless whether the Brownian motion behavior of particles is considered or not. The order of the magnitude is curve D > curve C > curve B > curve A. Since there is no energy barrier in case D, the number of particles collected for curve D is always greater than that of the three other interaction energy curves. Comparing curve A with curves B and C, even with the presence of the deep secondary minimum which will give rise to an accumulation of particles, the steepest slope between the secondary minimum and the primary maximum energy barrier of curve A is still the main reason why it has the lowest m value among these three curves. Because of a greater deposition probability caused by the normal convective force acting on those particles accumulated at the secondary minimum, the m value of curve C is higher than that of curve B. In addition, since the Brownian diffusion forces can help those particles to overcome the energy barrier shown in Fig. 2, so the m values for Brownian particles are greater than those of the non-Brownian particles as shown in Fig. 3.

Applying Eq. (4), the single collector efficiency η_s corresponding to those results obtained in Fig. 3, can be determined and are summarized in Table 2 and Table 3, respectively, for the cases of considering and without considering the Brownian motion behavior of particles. Similar to the results obtained in Fig. 3, the same order of the magnitudes of η_s for curves A–D are also observed in these two tables.

One of the potentially important features of the present Brownian dynamics simulation model is its capacity of providing detailed data about the morphology of the deposit based on the information of the position of the deposited particles. A typi-

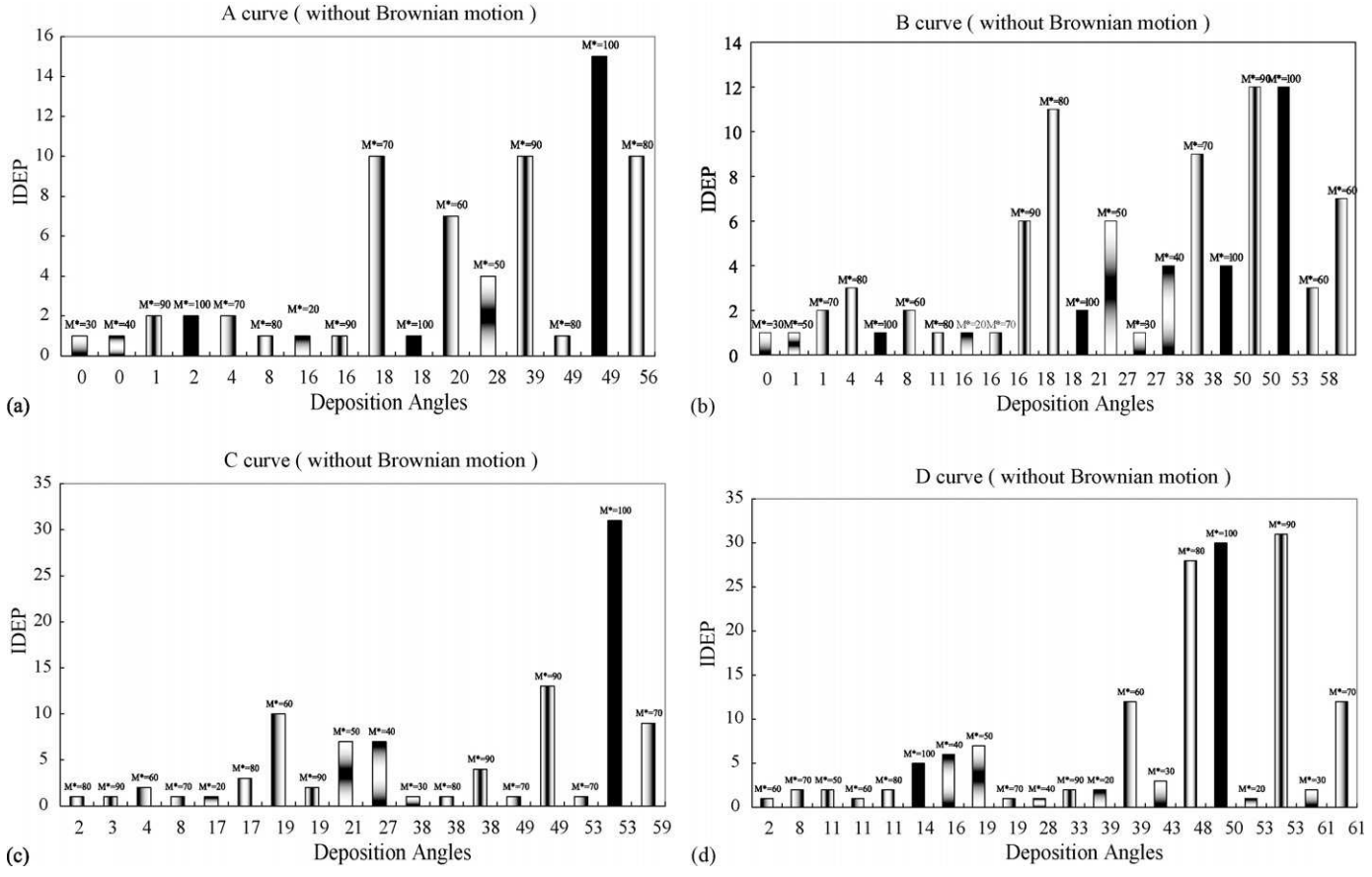

Fig. 6. Simulation results of m vs. the deposition angles at different M^* for all of the interaction energy curves shown in Fig. 2 when the Brownian motion behavior of particles is not considered: (a) the interaction energy curve A, (b) the interaction energy curve B, (c) the interaction energy curve C and (d) the interaction energy curve D.

cal set of simulation results for the deposition morphology of the interaction energy curve B is illustrated in Fig. 4(a) (non-Brownian particles) and Fig. 4(b) (Brownian particles), in which various values of $M^* = 20$, 40, 60, 80 and 100 are adopted. It can be found that the number of particles collected increases with an increase in M^*, and the Brownian particles always own a higher number of collections than that of the non-Brownian particles. Similar simulation results of the deposition morphology are obtained for the "barrierless" curve D as illustrated in Fig. 5(a) and (b), respectively. Apparently, the number of particles collected for curve D is greater than that of curve B.

In addition to the number of particles collected, another important feature concerned with the morphology of deposition is the angular position of those deposited particles. Based on the consideration of 40 approaching particles, the deposition angles of collected particles for all those four interaction energy curves shown in Fig. 2 are summarized in Fig. 6 (non-Brownian particles) and Fig. 7 (Brownian particles). As shown in Fig. 6, it can be found that those particles originating from the upstream control window have the tendency to concentrate their depositions near the location of $\theta = 20^\circ$ and of $\theta = 50^\circ$ (measured from the front stagnation point). For curves C and D where the primary maximum energy barrier do not existed, their favorable deposition angle $\theta = 50^\circ$ is greater than that of $\theta = 20^\circ$ for these two energy barrier existed curves A and B. When the Brownian motion behavior is considered as shown in Fig. 7, most of the approaching particles favor to deposit at locations near $\theta = 40^\circ$ and $\theta = 60^\circ$, which are greater than the case without considering the Brownian motion behavior as shown in Fig. 6. Also, as shown in both of these two figures, the angle of favorable deposition increases with the increase of M^*.

Corresponding to those simulation results obtained in Figs. 6 and 7, we had also estimated the shadow area cast by those particles deposited at different angles. The results are shown in Fig. 8(a)–(d). For curves A and B with the presence of the unfavorable energy barrier, it is found that the magnitudes of the shadow area increase with an increase of the deposition angle until the maxima are reached. Before these maxima, at a constant location of deposition, the shadow areas of Brownian particles are always larger than those of non-Brownian particles. This result indicates that particles with the Brownian motion behavior can form a larger dendrite on the collector surface than that of non-Brownian particles. Also, as shown in Fig. 8(a) and (b), the deposition angle corresponding to the maximum shadow area θ_{max} for the Brownian particles are smaller than that of non-Brownian particles, which indicates that Brownian particles have greater tendency to deposit at the front part of the collector than that of non-Brownian particles. For curve C as shown in Fig. 8(c), even with the same θ_{max}, the shadow areas of Brownian particles are always greater than those of non-Brownian

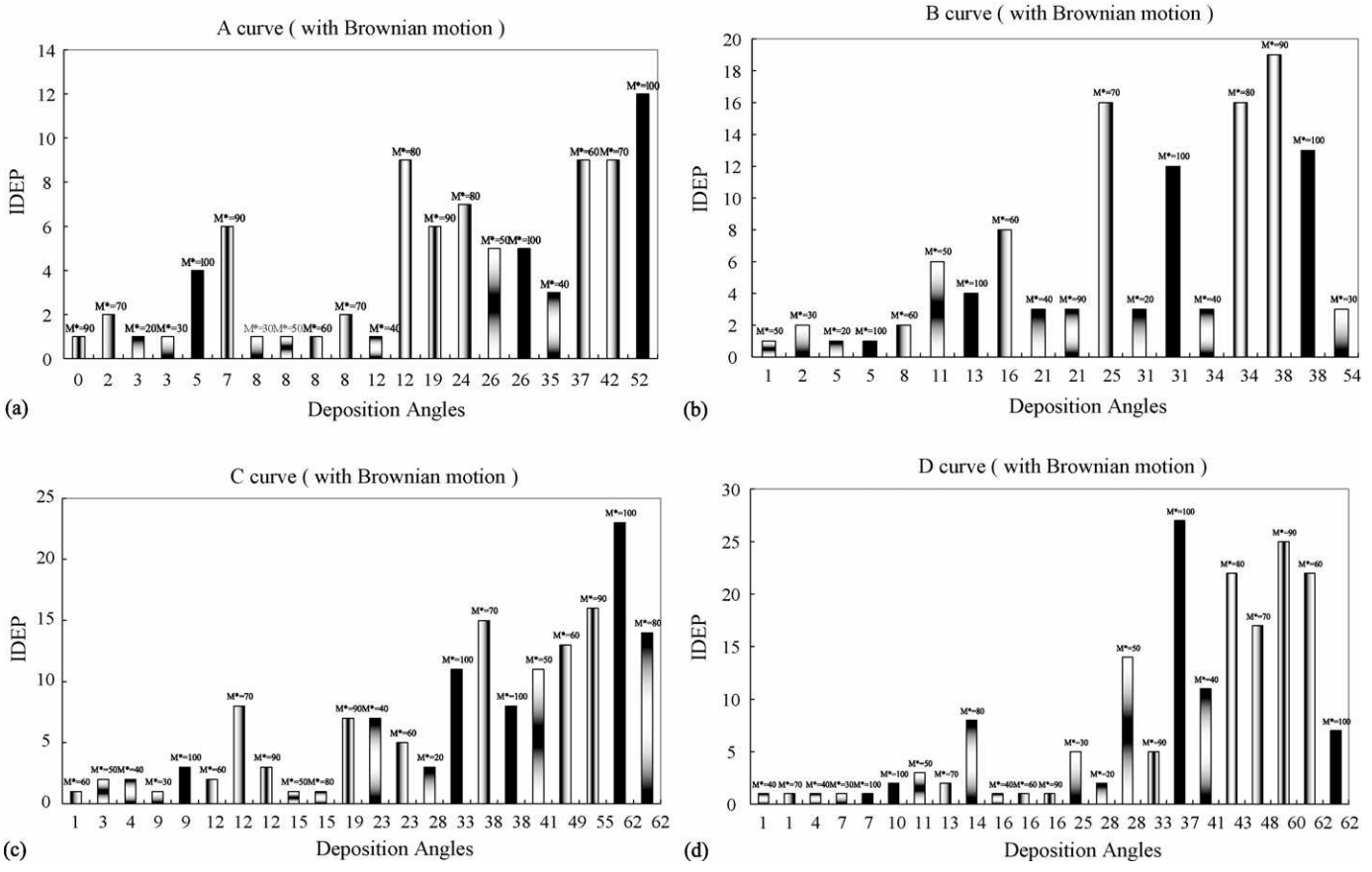

Fig. 7. Simulation results of m vs. the deposition angles at different M^* for all of the interaction energy curves shown in Fig. 2 when the Brownian motion behavior of particles is considered: (a) the interaction energy curve A, (b) the interaction energy curve B, (c) the interaction energy curve C and (d) the interaction energy curve D.

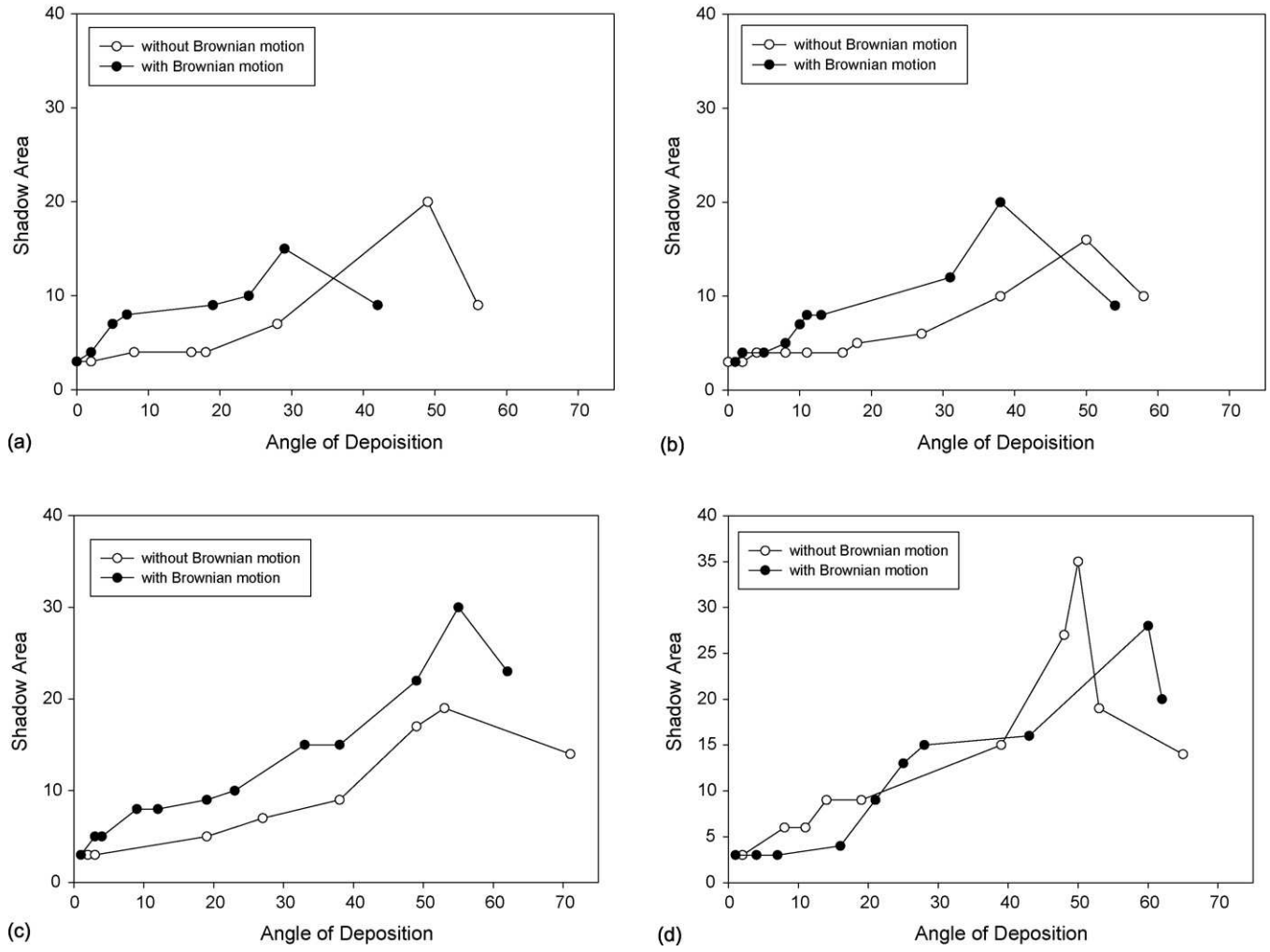

Fig. 8. The shadow areas cast by the particles deposited at different angles corresponding to those results obtained in Figs. 6 and 7 for all of the interaction energy curves shown in Fig. 2: (a) the interaction energy curve A, (b) the interaction energy curve B, (c) the interaction energy curve C and (d) the interaction energy curve D.

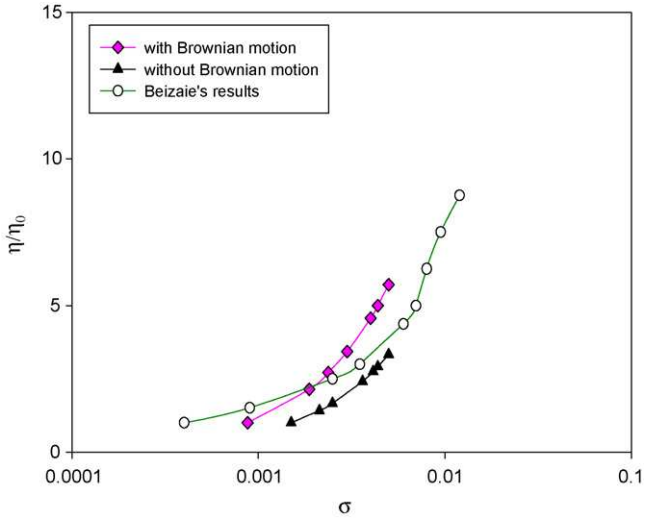

Fig. 9. Dependence of collection efficiency η_s/η_{s_0} on the amount of deposit σ for the spherical collector.

particles. On the contrary, for curve D where both the primary maximum and the secondary minimum do not existed, those non-Brownian particles can form a maximum area at a smaller angle than that of Brownian particles as shown in Fig. 8(d). In addition, it can be found that curve D always cause those deposited particles to exhibit the greatest area at different deposition angles among those four interaction energy curves shown in Fig. 2.

5. Conclusion

Applying the Brownian dynamics simulation method, the deposition morphology of Brownian particles onto a spherical collector for various types of the DLVO interaction energy curves has been studied. Both the singular and random motion behavior of approaching particles and the shadow effect of deposited particles are considered. The simulation results indicate that the Brownian particles can always cause a bigger shadow area at a smaller deposition angle than those non-Brownian particles. The particle's Brownian motion behavior can accelerate the formation of dendrites on the front part of

the spherical collector and therefore promotes the collection efficiency.

Because of its ability to describe the deposition process in a detailed step-by-step manner, the present stochastic simulation method can determine the collection efficiency as a function of the extent of particles efficiently. For example, if the extent of deposition is expressed in terms of m, then the increase of the collection efficiency can be written as

$$\frac{\eta_s}{\eta_{s_0}} = \frac{dm/dM^*}{(dm/dM^*)_{t\to 0}} \tag{13}$$

where η_{s_0} is the initial value of η_s. For a filter bed, one can define the volume of particles per unit volume of collector as

$$\nu = m\frac{4/3(\pi a_p^3)}{4/3(\pi a_c^3)} = mN_R^3 \tag{14}$$

and therefore the corresponding value of the specific deposit σ can be written as

$$\sigma = \nu(1-\varepsilon) \tag{15}$$

where ε is the filter porosity. By assuming $N_R = 0.05$ and the Stokes number of the approaching particle is zero, our simulation results of η_s/η_{s_0} versus σ are shown in Fig. 9. It can be found that the values of η_s/η_{s_0} increases with the increase of σ, and the values of Brownian particles are higher than those of non-Brownian particles. Our simulation results are also quite close to the results obtained by Beizaie et al. ([3], see case I in their paper), where the stochastic random motion behavior of Brownian particles was not considered in their trajectory equations.

Two other areas of study in which the present simulation method can be fruitfully applied are the investigation of the effect of poly-dispersity of particles and of the effect of the collector geometry (i.e. the constricted tube model established by Tien [4]) on the particle collection. The simulations for those two cases are being carried out at Tunghai University at the present time.

Acknowledgment

The financial support received from the National Science Council of the Republic of China, research grant no. NSC-94-2214-E-029-003, is greatly appreciated.

References

[1] C. Tien, C.S. Wang, D.T. Barot, Science 196 (1977) 983.
[2] C.S. Wang, M. Beizaie, C. Tien, AIChE J. 23 (1977) 879.
[3] M. Beizaie, C.S. Wang, C. Tien, Chem. Eng. Commun. 13 (1981) 153.
[4] C. Tien, Granular Filtration of Aerosols and Hydrosols, Butterworths, Boston, 1989, Chapters 3–5.
[5] C. Kanaoka, H. Emi, W. Tarthapanichakoon, AIChE J. 29 (1983) 895.
[6] D. Gupta, M.H. Peters, J. Colloid Interface Sci. 104 (1985) 375.
[7] B.V. Ramarao, C. Tien, S. Mohan, J. Aerosol Sci. 25 (1994) 295.
[8] Y.I. Chang, J.J. Whang, Chem. Eng. Sci. 53 (1998) 3923.
[9] Y.I. Chang, S.C. Chen, E. Lee, J. Colloid Interface Sci. 266 (2003) 48.
[10] B.V. Derjaguin, L.D. Landau, Acta Physicochim. 14 (1941) 733.
[11] IMSL Libraries, Houston, Texas, 1985.
[12] J.S. Kim, R. Rajagopalan, Colloids Surfaces 4 (1982) 17.
[13] A.C. Payatakes, H.Y. Park, J. Petrie, Chem. Eng. Sci. 36 (1981) 1319.